Research Paper

Multimodal analysis of aged wild-type mice exposed to repeated scanning ultrasound treatments demonstrates long-term safety

Daniel G. Blackmore[1,3], Fabrice Turpin[2,3], Abdalla Z Mohamed[2], Fangrong Zong[2], Rucha Pandit[1], Matthew Pelekanos[1], Fatima Nasrallah[2], Pankaj Sah[2], Perry F. Bartlett[1], Jürgen Götz[1✉]

1. Clem Jones Centre for Ageing Dementia Research, Queensland Brain Institute, The University of Queensland, Brisbane QLD 4072, Australia;
2. Queensland Brain Institute, The University of Queensland, Brisbane QLD 4072, Australia
3. These authors contributed equally to this paper.

✉ Corresponding author: j.goetz@uq.edu.au; Tel. +61.7.334.66329; Clem Jones Centre for Ageing Dementia Research, Queensland Brain Institute, The University of Queensland, Building 79, Upland Rd, Brisbane QLD 4072, Australia

Abstract

The blood-brain barrier presents a major challenge for the delivery of therapeutic agents to the brain; however, it can be transiently opened by combining low intensity ultrasound with microbubble infusion. Studies evaluating this technology have largely been performed in rodents, including models of neurological conditions. However, despite promising outcomes in terms of drug delivery and the amelioration of neurological impairments, the potential for long-term adverse effects presents a major concern in the context of clinical applications.

Methods: To fill this gap, we repeatedly treated 12-month-old wild-type mice with ultrasound, followed by a multimodal analysis for up to 18 months of age.

Results: We found that spatial memory in these aged mice was not adversely affected as assessed in the active place avoidance test. Sholl analysis of Golgi impregnations in the dentate gyrus of the hippocampus did not reveal any changes to the neuronal cytoarchitecture. Long-term potentiation, a cellular correlate of memory, was still achievable, magnetic resonance spectroscopy revealed no major changes in metabolites, and diffusion tensor imaging revealed normal microstructure and tissue integrity in the hippocampus. More specifically, all measures of diffusion appeared to support a neuroprotective effect of ultrasound treatment on the brain.

Conclusion: This multimodal analysis indicates that therapeutic ultrasound for blood-brain barrier opening is safe and potentially protective in the long-term, underscoring its validity as a potential treatment modality for diseases of the brain.

Key words: active place avoidance test, blood-brain barrier, diffusion tensor imaging, focused ultrasound, long-term potentiation

Introduction

Ultrasound is a highly versatile modality with the potential for treating diseases of the brain [1]. One increasingly pursued strategy is the delivery of ultrasound through the skull into the brain where the pressure waves interact with intravenously injected microbubbles. These are biologically inert and can either be generated in the laboratory or commercially sourced as clinically approved agents (under trade names such as Definity, Imagent and Optison) that are routinely used for contrast-enhanced ultrasound imaging. The microbubbles have a gas core that is encapsulated by a thin shell of lipid or polymer, with a diameter below 10 µm [2], i.e., within the range of the diameter of small blood vessels in the brain.

Interaction of the circulating microbubbles with ultrasound causes them to undergo cycles of compression and rarefaction. This results in transient opening of the blood-brain barrier (BBB), facilitated in part by the disruption of endothelial tight junctions, whereby therapeutic agents and other circulating factors in the blood can enter the brain parenchyma, eliciting a range of biological effects. In a series of studies, effective ultrasound parameters have been established for acoustic pressure [3-5], ultrasound frequency [3,5,6], pulse repetition frequency [7], pulse duration [7-9], and microbubble size [10]. Transient BBB opening has been demonstrated by the brain uptake of magnetic resonance imaging (MRI) contrast agents [11,12], fluorescently labeled dextrans of different sizes [13], and the dye Evans blue [14,15], all of which are normally excluded from the brain. Moving from these model compounds to therapeutic agents, there is an increased interest in developing therapeutic ultrasound into a treatment modality for neurological disorders including Alzheimer's disease, which has been the subject of many failed clinical trials based on conventional approaches [16].

The Alzheimer's disease brain is characterized by both amyloid-β (Aβ) and tau pathology [17]. Ultrasound-mediated BBB opening (termed obicodilation by us [1]) has proven effective and safe in removing toxic protein aggregates in a range of Alzheimer's mouse models, either on its own [15,18-21], or in combination with a therapeutic antibody targeting Aβ or an antibody fragment targeting tau [20,22]. In a subset of these studies, reducing pathological forms of Aβ and tau was shown to be associated with a concomitant improvement in memory functions [15,19,20]. Some of these studies targeted small areas of the brain, whereas we have also investigated a scanning ultrasound (SUS) mode that opens the BBB transiently over the entire brain [15,20,21]. Our rationale was that amyloid and tau pathology is found throughout the Alzheimer's brain, with only the cerebellum being spared until late in the disease [17], suggesting that large parts of the forebrain would need to be sonicated to achieve a therapeutic outcome. It is therefore critical to use a wide range of structural and functional readouts (see below) to broadly examine the effects of BBB opening when treating larger areas of the brain.

These proof-of-principle studies demonstrated that therapeutic ultrasound treatment of mice is an effective procedure to clear toxic protein accumulations in the brains of Alzheimer's disease models and to improve cognitive functions. The studies also addressed safety aspects of the treatment, with no adverse impact found on neuronal tissue when using predominantly histological methods.

Safety studies were also performed in wild-type mice, again mostly using histological readouts [3,4,7,8]. Even biweekly sonication of the striatum over five months was found to cause no overt damage [23], although performing a second BBB opening within 20 min has been reported to cause a nearly twofold increase in extravasation of albumin bound to Evans blue [24]. Importantly, safety studies have also been extended to larger animals. These include aged beagles (9-11 years old) [25] that received either a single treatment or weekly treatments over the course of four weeks, targeting a defined area of the brain. The applied power was determined by a ramp-up protocol with ultraharmonic detection. Safety was demonstrated by acquiring T2- and T2*- weighted images post-treatment, running a neurological test battery, and determining that there were no changes in the number of microhemorrhages in brain tissue taken after sacrifice [25]. In another study, three- to eight-year-old sheep also underwent sonications, assessing multiple single treatments with a range of pressures [26]. BBB opening was monitored post-treatment via Evans blue extravasation and endogenous IgG uptake, and staining with either hematoxylin & eosin (H&E) or vanadium acid fuchsin stain was used to assess cell damage and red blood cell infiltration [26]. In a study in macaques of unspecified age, the commercial ExAblate 4000 low-frequency TcMRgFUS system (InSightec) was used and was integrated with a clinical 3 T MRI unit [27]. BBB opening was monitored by MRI using gadopentetic acid and exposures were assessed by using passive cavitation as a guide to reduce the power when a certain threshold was reached. T2*-weighted images were acquired post-sonication. Safety was demonstrated behaviorally by evaluating visual acuity and higher-order cognitive abilities using touch screens, as well as by subsequent histological analysis [27]. Similarly, in another macaque study, no impairment was found in decision-making and motor control after opening the BBB [28]. Finally, in a first-in-human safety trial exploring BBB opening as a potential avenue to treat Alzheimer's disease, five patients were enrolled, with a mean age of 66 years [29]. These patients underwent one or two sonications targeting the right frontal cortex. MR thermometry was used to monitor tissue temperature at the sonicated region in real time. After completion of the sonication protocol, a gadolinium-enhanced T1 sequence was performed to verify BBB opening. Additional high-resolution MRI sequences were obtained post-sonication, and the patients were admitted to the surgical short stay unit for overnight observation, demonstrating safety in Alzheimer's disease patients. Together these findings

demonstrate that ultrasound is a potentially safe method to open the BBB in multiple areas in multiple species, including humans [29].

Although a note of caution has been raised following the demonstration of sterile inflammation induced by BBB opening in rats [30], a subsequent study using a different type and concentration of microbubbles did not find a damaging inflammatory response [31]. In other words, as for the ultrasound parameters, microbubble dosing can be optimized to achieve biological outcomes without compromising safety. We recently added an electrophysiological component to the safety analysis and revealed that ultrasound neither impaired neuronal excitability nor adversely affected dendritic morphology in wild-type mice in which weekly SUS treatments were initiated at four months of age for six weeks, followed by sacrifice of the animals three months later [32].

However, when considering clinical applications for age-dependent chronic brain diseases, it is important to test older animals and assess longer term outcomes. In the current study, we initiated weekly sonications in 12-month-old wild-type mice, the age at which they start to cognitively decline [33], and then analyzed the effects at 15 and 18 months of age. This age bracket reflects the age of human patients who would likely participate in Alzheimer's disease therapeutic intervention trials. Moreover, histological and electrophysiological studies provide only a snapshot of brain function. As our SUS treatment opens the BBB over the entire brain [15,20,21] it is vital to test the impact of this procedure on overall neural function.

We therefore performed a multimodal analysis that included the assessment of spatial memory using the active place avoidance (APA) test, field recordings to assess basal synaptic transmission and long-term potentiation (LTP), which is the molecular mechanism underlying memory formation, and Golgi staining to address neuronal morphology. The close association of hippocampal function with memory performance further prompted us to measure profiles of key metabolites using proton magnetic resonance spectroscopy (^{1}H-MRS). *In vivo* diffusion tensor imaging (DTI) was also performed to determine tissue integrity and microstructure. Several of these analyses focused on the hippocampus, the region of the brain that undergoes functional impairment and neurodegeneration early in Alzheimer's disease [34]. With translation to human studies in mind, additional analyses were performed in live animals prior to sacrifice for electrophysiological and histological analyses. Taken together, these approaches allowed us to examine whether SUS treatment adversely affects long-term functional and cognitive outcomes, including spatial learning, in wild-type mice of advanced age.

Methods

Animal ethics

All experimental procedures in this study were approved by the University of Queensland Animal Ethics Committee (QBI/412/14/NHMRC). Experiments were conducted in compliance with the ARRIVE guidelines (Animal Research: Reporting in Vivo Experiments) for how to report animal experiments. Mice were maintained on a 12 h light/dark cycle and housed in a PC2 facility with *ad libitum* access to food and water. Female C57Bl/6 mice were used in this study to minimize unused animals in our breeding colony in accordance with the guidelines of the Australian Code of Practice for the Care and Use of Animals for Scientific Purposes. Previous studies have determined that female C57Bl/6 mice become acyclic at 10 months of age, ruling out potential confounding effects of the estrous cycle [32].

Study design

The study included a total of 24 mice in which sonication was initiated at 12 months of age. The mice were tested in the APA test with random allocation and then treated weekly over 6 weeks with SUS or sham (n=12 SUS/12 sham). At 15 months, the mice were retested in the APA test (12/12). At 18 months, the mice were again tested in the APA test (11 as one suffered an eye tumor/12). A total of 18 mice (8/10) underwent MRI scanning. Two mice, one in each group, died during the scanning procedure due to the effect of anesthesia and were excluded from the study (7/9). Anatomical MRI (voxel-based morphometry, VBM) (7/9), MRS (7/9) and DTI (7/9) data were acquired. A subset of the animals was then sacrificed, and brain slices were taken and analyzed for LTP in the dentate gyrus (4/5). The subset of mice that did not undergo MRI and electrophysiological analysis was used for Golgi staining of the dentate gyrus (3/3; 25 neurons each) (**Figure 1**). The experimenters were blinded to the treatment conditions. To demonstrate BBB opening throughout the majority of the brain, 12-month-old C57Bl/6 mice (3/2) were used. Additional C57Bl/6 mice (n=5 for two SUS groups, aged 15 months) were used in the work-up of BBB opening to achieve unilateral targeting of the hippocampus.

SUS equipment

An integrated focused ultrasound system (Therapy Imaging Probe System, TIPS, Philips Research) was used [35]. The TIPS system consists of

an annular array transducer with a natural focus of 80 mm, a radius of curvature of 80 mm, a spherical shell of 80 mm with a central opening of 31 mm diameter, a 3D positioning system, and a programmable motorized system to move the ultrasound focus in the x and y planes to cover the entire brain. A coupler mounted to the transducer was filled with degassed water and placed on the head of the mouse with ultrasound gel for coupling (**Figure 1**). The focal zone of the array was an ellipse of approximately 1.5 mm × 1.5 mm × 12 mm.

Production of microbubbles

Lipid-shelled microbubbles with an octafluoropropane core were manufactured and characterized in-house. A 1:5:2:1 mass ratio of PEG6000, distearoyl-phosphatidylcholine, distearoylphosphatidylethanolamine, and pluronic F68 was dissolved in a 0.9% solution of sodium chloride. The solution was added to glass high-performance liquid chromatography (HPLC) vials and the air was removed and replaced with octafluoropropane gas to fill the headspace of the vial (Arcadophta). On the day of use, the vials were heated to room temperature and then shaken in a dental amalgamator for 40 s at 4,000 rpm. Microbubble characterization was performed using a Coulter counter (Multisizer 4e, Beckman Coulter Life Sciences) with a 30 μm aperture. Activated microbubbles were diluted 1:5,000 in diluent (IsoFlow, Beckman Coulter Life Sciences), and blank measurements were done with a microbubble solution that had been sonicated for 10 s in an ultrasonic cleaner.

SUS and sham application

Mice were anesthetized with ketamine (100 mg/kg) and xylazine (10 mg/kg), after which they were shaved and the hair on their head was depilated. The mice were then injected retro-orbitally with 1 μL/g body weight of microbubble solution and placed under the ultrasound transducer with their head immobilized. Ultrasound gel was used to seal all interfaces between the head and transducer to eliminate air gaps. The mice received sonications using the following parameters: 1 MHz center frequency, 0.7 MPa peak rarefactional pressure, 10 Hz pulse repetition frequency, 10% duty cycle, and 6 s sonication per location. The motorized positioning system moved the focus of the transducer array in a grid with 1.5 mm between individual sites of sonication so that ultrasound was delivered sequentially to the entire brain (hence scanning ultrasound, SUS). For sham treatments, mice went through the entire procedure including microbubble injections, but no ultrasound was delivered. Micro-bubble injection and SUS starting position were alternated weekly between the mouse's left and right sides.

Visualization of BBB opening and assessment of tissue damage using H&E staining

To visualize widespread BBB opening following whole-brain SUS, mice (n=3) were SUS-treated as above (using sham treatment as the control, n=2) and injected with 30 μL Evans blue dye (E2129, Sigma, 2% in saline) immediately after the sonication. The mice were sacrificed by transcardial perfusion 60 min after sonication, after which their brains were fixed in 4% paraformaldehyde (PFA) overnight, cut coronally to 1 mm in a brain block, and imaged at 700 nm for 30 s in a fluorescence scanner (Odyssey Fc, LI-COR). To detect microhemorrhages, hippocampal slices were then paraffin-embedded and sliced at 7 μm, before being stained with H&E and microscopically examined for extravasated erythrocytes, which stain bright red. In cases where only the hippocampus was targeted, a total of 10 mice were anesthetized by inhalant isoflurane. The focus of the transducer array was moved to target the left hippocampus using stereotaxic coordinates. Together with the microbubbles (1 μL/g), fluorescein-labeled 3 or 70 kDa dextran (Thermo Fisher Scientific, D1822) was injected retro-orbitally (n=5 mice in each case). Parameters used for
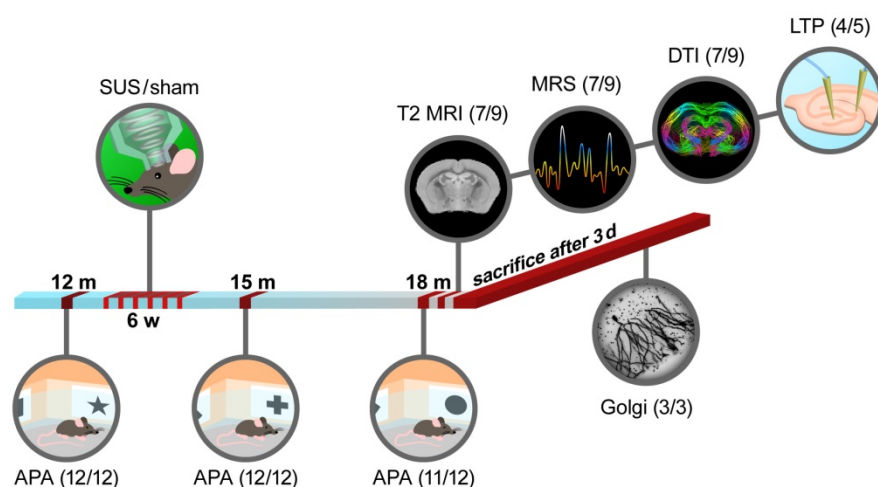

Figure 1. Study design for the multimodal long-term safety analysis of SUS-treated aged wild-type mice. Scheme of sonication set-up and experimental procedure.

ultrasound delivery were as above, except for a 1 min sonication time and a 1.5 MHz center frequency. The mice were allowed to recover from anesthesia and were sacrificed 60 min after sonication, transcardially perfused with 4% PFA and their brains sectioned at 100 μm thickness on the following day. The sections were serially mounted and imaged as whole brain sections at a 10X magnification.

Active place avoidance test

The APA task is a test of hippocampus-dependent spatial learning in which animals are placed in a rotating arena and trained to actively avoid a shock zone (1/6 of the total surface, see below) using visual cues [36]. The mice were tested over five days in a rotating elevated arena (Bio-Signal Group) that had a grid floor with a 32 cm high clear plastic circular fence 77 cm in diameter. High-contrast visual cues were present on the walls of the testing room. The arena was rotated at a speed of 1 rpm and a 500 ms, 60 Hz, 0.5 mA mild shock was delivered through the grid floor when the animal entered a 60° shock zone, and every 1,500 ms until the animal left this zone. The shock zone was maintained at a constant position in relation to the room. Recorded tracks were analyzed with Track Analysis software (Bio-Signal group). Animals underwent a habituation session 24 h before the first training session, in which they were placed in the rotating arena for 5 min to explore but did not receive any shocks. After the initial testing phase, the mice were divided into two groups with the animals matched across the groups so that their performance on day five of the task was the same. Five training sessions were held on consecutive days, one per day with a duration of 10 min.

Following a 6-week period of treatment in which the mice were given SUS or sham treatment, the animals were housed in groups of four until being retested 1.5 months later (reversal learning, with the animals now being 15 months old). For retesting, the shock zone was switched to the opposite side of the arena and the visual cues were changed but the mice were tested in the same room. As before, animals were tested during five training sessions conducted on consecutive days. The number of shocks delivered to the SUS-treated mice and the sham-treated mice were compared over the days of testing. A final APA test was conducted 6 months after the original test (18 months of age) in order to determine if there was any long-term effect of SUS treatment on aged animals. In this final task, animals were tested in a novel room with novel spatial cues. In all behavioral tests, examiners were blinded to treatment. Data were analyzed with a two-way ANOVA, with day of

testing as a within-subjects factor and simple effects of group tested with the Bonferroni *post-hoc* test.

In vivo magnetic resonance imaging

In vivo MRI scans were acquired on a 16.4 T Bruker system (Ultrashield 700 QB Plus; vertical bore interfaced to the Paravision software PV6.0.1). The mice were vertically positioned in the scanner. They were initially anesthetized by inhalation using a mixture of oxygen and 3-4% isoflurane and then maintained using 1.5-2.5% isoflurane. An MR-compatible small-animal monitoring system was used to monitor the respiration rate continuously throughout the entire experiment (SA Instruments Inc.). The rectal temperature was monitored throughout the whole scanning session and maintained at 36±1 °C using a water-circulated heating pad, with respiration also monitored continually (75-90 bpm).

The optimized MR protocol consisted of an axial, coronal and sagittal T2 rapid acquisition with a relaxation enhancement (Turbo-RARE) scan (RareFactor = 4, TR = 7,500 ms; TE = 12 ms; averages = 2; field of view = 16×20 mm, slice thickness = 0.5 mm). Coronal and sagittal T2 scans were mainly rapid acquisitions to assist in the positioning of voxels for the ^{1}H-MRS. For the DTI, a spin-echo sequence with interleaved slice acquisition using TR/TE = 6,000/14.15 ms was acquired. Diffusion sensitizing gradients were applied in 30 non-collinear, uniformly distributed directions with the gradient strength b = 1500 s/mm^2, acquiring two images with the b-value set to '0' (b_0). The acquisition matrix was 133×120 over a field of view of 20×18 mm^2 to produce a final in-plane resolution of 150×150 μm^2, with a 0.6 mm slice thickness. The number of excitations and the partial Fourier encoding acceleration were set to 1.6 and a total number of 2 averages. The total acquisition time was 2 h. All images were acquired with respiratory gating.

For the *in vivo* ^{1}H-MRS, adjustments of all first- and second-order shims over the voxel (i.e., volume) of interest were accomplished with the FASTMAP procedure. Typically, the *in vivo* shimming procedure resulted in an approximately 50 Hz full-width half maximum line-width of the unsuppressed water peak over the spectroscopy voxel. Spectroscopy data were collected using a short-TE point-resolved spectroscopy (PRESS) sequence (TR = 5,000 ms, TE = 20 ms, 320 averages, 2,048 complex data points with a spectral width of 10,000 Hz). The water signal was suppressed with variable power radio frequency pulses with an optimized relaxation delay (VAPOR) technique interleaved with the outer volume saturation (OVS) modules. This PRESS sequence was

used for MRS data acquisition from the cortex (voxel volume = 4×2×0.9 mm³) and the hippocampus (voxel volume = 2×1×2 mm³). The acquisition time for each voxel of interest was 26 min.

Magnetic resonance imaging data analysis

T2-weighted images were reoriented to have the correct labeling and skull stripping to extract the brain using the pulse-coupled neural networks (PCNN) protocol [37], followed by N4 field bias correction to correct for field inhomogeneity [38]. Images were then registered linearly and nonlinearly using the FMRIB linear co-registration tool (FLIRT) [39,40] and the FMRIB nonlinear co-registration tool (FNIRT) [41], respectively, to the template provided by the Australian Mouse Brain Mapping Consortium (AMBMC) [42,43]. Jacobian maps were calculated and used for the VBM analysis between the SUS and sham groups. VBM analysis steps were processed as previously reported [44]. T2 images were registered to the AMBMC template through the VBM analysis package available in the FSL Imaging Analysis Suite, comparing the SUS with the sham group.

DTI data were motion-corrected using FSL-MCFLIRT [39] with the b0 volume as a reference, skull-stripped using the PCNN protocol function and then refined and modified manually. N4 bias field correction was performed to correct for field inhomogeneity. The FSL Diffusion Toolkit (Dtifit) was used for local fitting of diffusion tensors and to generate a series of maps [45]. DTI parametric maps were registered to the AMBMC mouse template by linearly registering the b0 image to T2-RARE using the FLIRT function.

Quantification of the MRS data was based on a frequency domain analysis using 'Linear Combination of Model spectra' (LCModel) [46]. *In vivo* spectra were analyzed by superposition of a simulated basis dataset provided by the LCModel software. The water signal served as a reference for determining the metabolite concentration, which was acquired from the same voxel. The metabolic profile was measured with the same parameters except that the number of averages was set to 320. The results were normalized by the LCModel package and reported relative to the concentration of the creatine peak.

To compare the SUS and sham groups, we conducted unpaired 2-sample t-tests using FSL-randomize [47] for nonparametric permutation tests with 1,000 permutations function and corrected for multiple comparisons using a threshold-free cluster enhancement correction with z = 2.3, p < 0.05 and a cluster size of 30 voxels.

Electrophysiology

Mice were deeply anesthetized with isoflurane, perfused transcardially with ice-cold cutting solution (in mM: 93 NMDG, 2.5 KCl, 1.2 NaH$_2$PO$_4$, 30 NaHCO$_3$, 20 HEPES, 25 glucose, 5 sodium ascorbate, 2 thiourea, 3 sodium pyruvate, 10 MgSO$_4$, 0.5 CaCl$_2$; pH 7.3 adjusted with HCl; osmolarity 300-310 mOsm/kg) and subsequently decapitated. The brain was rapidly removed and 400 µm coronal brain slices were prepared in ice-cold cutting solution using a Leica VT1000S vibratome. The slices were allowed to recover in oxygenated artificial cerebrospinal fluid (aCSF; in mM: 118 NaCl, 25 NaHCO$_3$, 10 glucose, 2.5 KCl, 1.2 NaHPO$_4$, 1.3 MgCl$_2$, 2.5 CaCl$_2$) for 30 min at 32 °C and then equilibrated to room temperature for 30 min. Slices were visualized using an upright microscope (Olympus BX50WI), and field potentials were recorded using a Multiclamp 700B amplifier (Molecular Devices). During recording, slices were perfused with heated aCSF (30±2 °C) and GABAergic activity was blocked by bath application of picrotoxin (100 µM, Tocris). Recording pipettes were prepared from borosilicate glass (GC150F, Harvard Apparatus) and pulled to a tip resistance of 3-6 MΩ (Narishige PC-10) when filled with aCSF. Local electrical stimulation of the medial perforant pathway was evoked using a theta glass pipette. LTP was induced by a theta burst protocol (10 trains at 5 Hz with 10 pulses at 100 Hz repeated 3 times, 20 s apart). During baseline and after theta burst stimulation, field excitatory post-synaptic potentials (fEPSPs) were evoked every 30 s.

Golgi staining

The Golgi-Cox method was applied as previously described [48]. Briefly, mice were deeply anesthetized with sodium pentobarbitone (Lethobarb) and perfused transcardially with a 0.9% saline solution followed by 0.4% paraformaldehyde. Dissected brains were immersed in the Golgi-Cox solution for a week, with the medium being replaced after the first 24 h. Subsequently, brains were washed twice in distilled water, immersed for 40 min in 30% ammonia solution, and washed again in distilled water twice for 5 min. The brains were then immersion-fixed in 5% sodium thiosulfate solution for 10 min, after which they were sliced coronally at a thickness of 150 µm. The sections were then mounted on gelatinized slides and processed through dehydration steps in 50, 75, 95 and 100% ethanol for 4 min each. Finally, the sections were cleaned with xylene for 2 h. A Sholl analysis was performed to determine the number of intersections, the total number of terminals per cell, the node distribution over the dendrites, and the total number of nodes per

cell.

Results and discussion

Six weekly SUS treatments initiated at 12 months do not impair spatial learning at either 15 or 18 months of age

To assess the long-term safety of ultrasound treatment, we performed a multimodal analysis that involved an assessment of spatial memory at 12 months, followed by six weekly SUS treatments (microbubble injection and SUS under anesthesia, n=12), using sham treatments (microbubble injection without SUS under anesthesia, n=12) as the control. This was followed by a second assessment of spatial memory at 15 months, and a multimodal analysis including spatial memory assessment at 18 months (**Figure 1**).

The study was initiated at 12 months as previous studies in female C57Bl/6 mice had demonstrated that cognitive functions begin to deteriorate around this age [33]. No study has previously assessed the impact of SUS against a backdrop of cognitive decline to understand whether the procedure is safe to apply in the intended Alzheimer's clinical population, which presents with cognitive deficiencies. Spatial learning could have been assessed in the Morris water maze; however, this test is stressful to mice [49], and aged animals tend to float during the task [50]. Instead, the hippocampus-dependent APA paradigm was chosen, a test which we had previously demonstrated to be suitable for assessing the impact of ultrasound-mediated BBB opening on cognition in Alzheimer's mice [15]. Baseline spatial memory was assessed at 12 months of age using the APA test. As expected, all mice performed well over a five-day trial as shown by a reduction in the number of shocks received (**Figure S1A**), increases in the maximum time spent avoiding the shock zone (**Figure S1B**), and the time to first shock (**Figure S1C**) during each day of the test period. Improvement during the test period was also examined by comparing the number of shocks received on the first day to that on the final day of testing for each animal and represented as a percentage) with no difference observed between the two groups (**Figure S1D**).

We next performed SUS, using sham treatments as a control (**Figure 1**). Coulter counter measurements showed our in-house-made microbubbles had an average size of 1.35 μm, with 90% being between 0.76 and 2.01 μm in diameter, and a concentration of 1.7×10^9/mL (**Figure 2A**). The sonication parameters chosen for the SUS group have been shown to produce widespread opening of the BBB, as demonstrated by extravasation of albumin carrying

Evans blue [15,20,21]. A single sonication of 12-month-old mice using the SUS protocol achieves widespread opening that includes the hippocampus, the function of which we mainly assessed as they are among the first to deteriorate in Alzheimer's disease [51]. BBB opening was confirmed by imaging 1 mm coronal slices of brains from SUS- and sham-treated mice for extravasated Evans blue dye. Far-red (700 nm) scans revealed that the maximal fluorescence intensity of the SUS-treated brains was approximately 5-fold greater than that of sham-treated mice (**Figure 2B**). Histological examination of sections from hippocampal areas in the three SUS-treated mice revealed no evidence of microhemorrhages, as indicated by H&E staining (**Figure 2C-D**). We also used fluorescently labeled 3 kDa and 70 kDa dextran to demonstrate targeted BBB opening of the left hippocampus (with the right, non-targeted hippocampus as a control) at 15 months of age (**Figure 2E-F**), again without causing any overt damage (data not shown). Having shown that we were able to consistently open the BBB either in a targeted manner or throughout the brain, we performed six weekly SUS and sham treatments in the 24 wild-type mice that had undergone the APA test.

We were encouraged in performing multiple treatments at this age, as we had previously used histological readouts to demonstrate that between 4 and 7 SUS treatments are well tolerated in mice up to an age of 22 months [15,21]. Six weeks after the final SUS or sham treatment, when animals were 15 months old, they were retested using the same behavioral test. This revealed that the SUS-treated animals initially received more shocks than the sham-treated animals; however, this was only significant on day 2 and by the final day of testing there was no difference in shock numbers between the two groups (**Figure S2A**). There was also no significant difference between groups in the maximum time spent avoiding the shock zone (**Figure S2B**) or time to first shock (**Figure S2C**), and both groups demonstrated comparable improvement during the APA test period (**Figure S2D**). Again, this was calculated by comparing the number of shocks received on the first day to that on the final day of testing for each animal and representing this value as a percentage. There was also no difference in the speed or distance travelled during testing (data not shown), demonstrating that the SUS treatment had no adverse effects on the aged animals.

Finally, six months after the original APA test, all animals, now aged 18 months, were re-tested a second time. Although this is an age of considerable decline and metabolic changes [52], the final round of spatial learning again revealed no significant differences in

shock numbers between treatment groups (**Figure 3A**), maximum time avoiding the shock zone **(Figure 3B)**, or time to first entrance of the shock zone **(Figure 3C)**. Furthermore, when we compared the learning ability during the course of the test period there was no significant difference between groups (**Figure 3D**). When examining the performance of animals on an individual basis, it was noted that three of the sham-treated animals performed more poorly on the last day of than on the first day in terms of shocks received (**Figure 3E**), compared to only one animal in

the SUS-treated group (**Figure 3F**). This is in agreement with our previous work, which has shown that six weekly SUS treatments have a protective effect, maintaining dendritic length and complexity, which may allow improved connectivity in the hippocampus and thus have a role in maintaining cognitive function [32]. Taken together, these results demonstrate that SUS treatment initiated at 12 months of age did not adversely affect spatial learning at any of the ages analyzed.
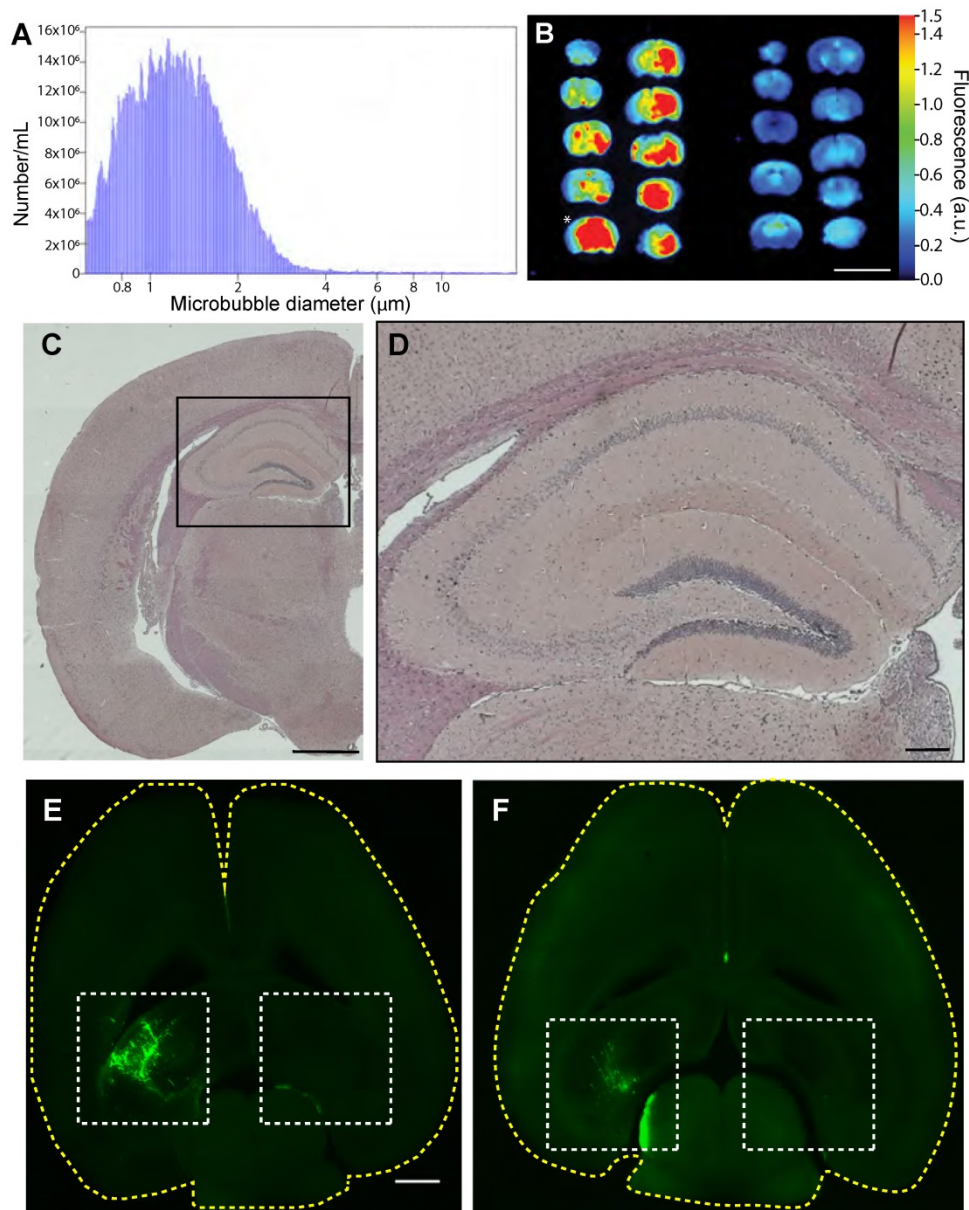

Figure 2. SUS treatment of aged mice using in-house microbubbles allows for widespread BBB opening without hemorrhaging. (A) Size distribution plot of in-house-made microbubbles determined by Coulter counter. Microbubble diameters are grouped into 0.046 mm bins, and the number /mL is the count per bin. **(B)** 700 nm fluorescence intensity image of Evans blue uptake in a mouse brain (1 mm coronal slices) treated with SUS at 12 months (left) compared to the sham control (right). Heat map in arbitrary units (a.u.) compared to background. Scale bar: 10 mm. * indicates slice used for histological section. **(C-D)** Hematoxylin & eosin staining of sections taken from SUS-treated mice demonstrates absence of hemorrhages in the hippocampus (at low (C), and high (box, D) magnification). **(E-F)** Visualization of the opening of the BBB in 15-month-old mice (horizontal sections) in which fluorescently labeled 3 kDa (E) and 70 kDa dextran (F) was used to demonstrate targeted BBB opening of the left hippocampus (with the right, non-targeted hippocampus as control). Scale bar: 1 cm (B), 1 mm (C, E), 200 μm (D).
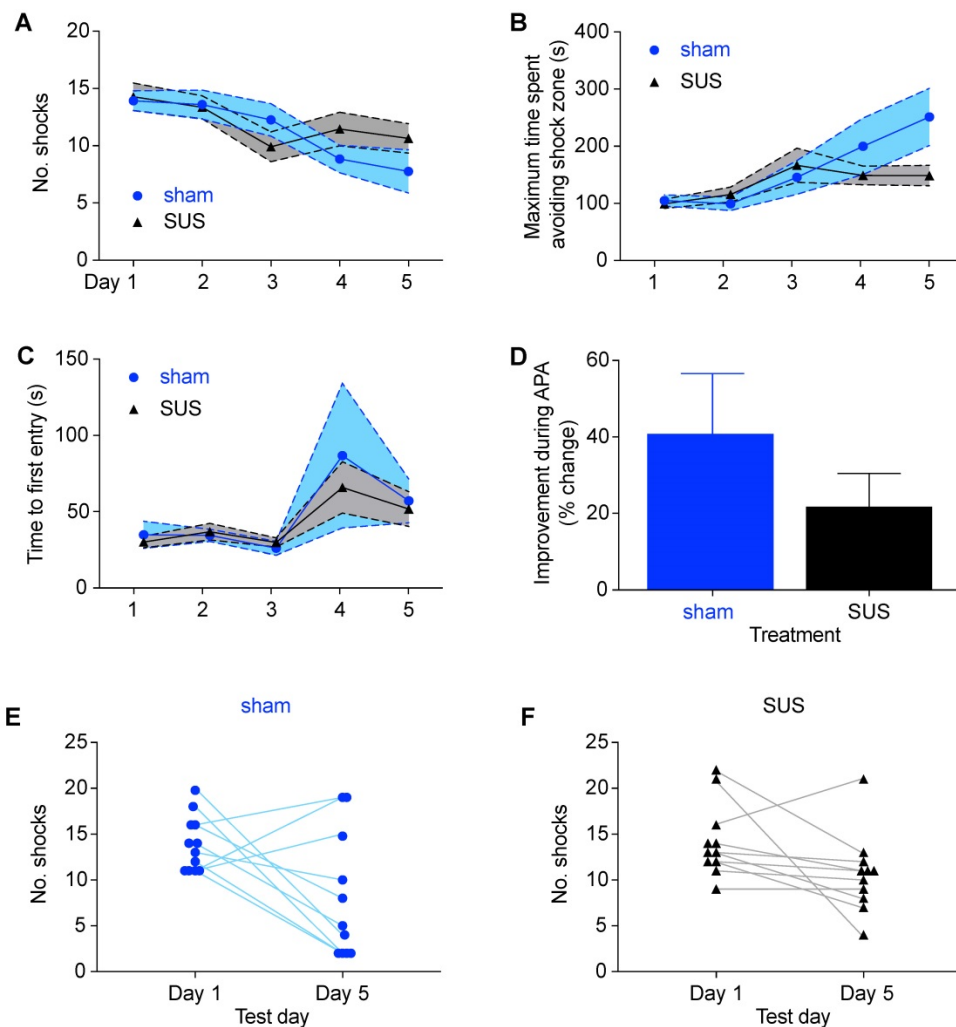
Figure 3. SUS treatment does not adversely affect spatial learning in 18-month-old mice. (A) No significant difference in shock number during each day of testing was detected between the SUS- and sham-treated groups in the final round of APA testing 6 months after SUS treatment was initiated (mean ± SEM represented as a shaded area contained within dotted lines). There was also no difference between SUS- and sham-treated groups when comparing maximal time spent avoiding the shock zone (**B**) or the time to first entrance of this zone (**C**) during the course of APA testing (mean ± SEM represented as a shaded area contained within dotted lines; two-way ANOVA with Bonferroni post-hoc test). (**D**) The learning ability did not differ between the groups (mean + SEM; student's t-test, n.s.). Individual comparison of the number of shocks received on the first and last day for each animal showed that three animals in the sham-treated group received more shocks (**E**) versus only one in the SUS-treated group (**F**) on the final day of testing.

SUS treatments initiated at 12 months of age do not alter metabolites at 18 months

The C57BL/6 mouse brain is known to be associated with volume changes during aging, in particular in the striatum and hippocampus [53]. At 18 months of age, we applied a VBM analysis to 7 SUS- and 9 sham-treated mice but saw no differences between the groups.

Metabolites are considered the building blocks of neurons, with their changes reflecting altered cellular function. For instance, myo-inositol is a marker for Alzheimer's disease pathology, and N-acetylaspartate and glutamate both decrease in transgenic Alzheimer's mouse models in an age-dependent manner [54,55]. To evaluate the safety of SUS, we therefore measured these and other metabolites by *in vivo* ^{1}H-MRS, analyzing the acquired time-domain data with the LCModel [46]. Axial anatomical images of two spectroscopic voxel locations, the cortex and the hippocampus, are illustrated (**Figure 4A-B**). A number of metabolites could be reliably detected in the spectra across all animals, including creatine, phosphocreatine, glutamate, glutamine, glycerylphosphorylcholine, glutathione, N-acetylaspartate, N-acetylaspartylglutamate, and taurine. The data were subsequently subjected to one-way ANOVA and a two-sampled unpaired t-test, with the boxplots for the prefrontal cortex presented in **Figure 4C** and those for the hippocampus in **Figure 4D**. N-acetylaspartate was significantly decreased in the cortex, but not the hippocampus of the SUS group. There were no significant changes in the other metabolites.
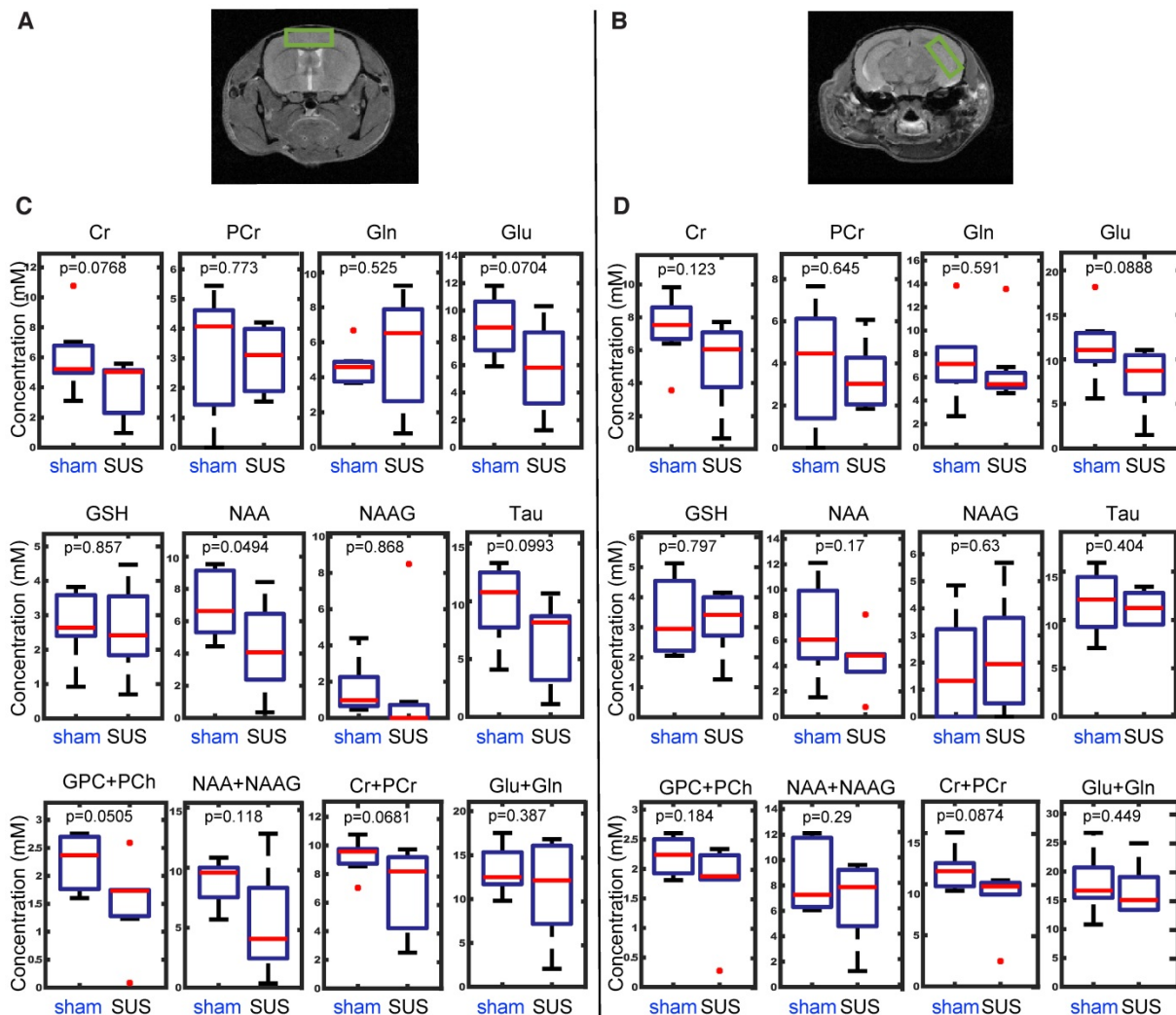
Figure 4. *In vivo* ¹H-MRS reveals no differences in metabolite concentrations between SUS- and sham-treated mice in either the cortex or hippocampus. Axial anatomical images of two spectroscopic voxel locations, the cortex (A) and the hippocampus (B). Boxplots representing differences in metabolite concentration from a region of interest taken in the cortex (C) and hippocampus (D). Metabolites: creatine (Cr), phosphocreatine (PCr), glutamate (Glu), glutamine (Gln), glycerylphosphorylcholine (GPC+PCh), glutathione (GSH), N-acetyl-aspartate (NAA), N-acetylaspartylglutamate (NAA + NAAG), and taurine (Tau).

SUS treatments alter diffusion measures at 18 months

DTI is considered a marker of tissue microstructure as it detects changes in water diffusion properties [56-59]. Such changes are likely to manifest as an increase in tissue density (due to reshaping of neuronal or glial processes), or an enhancement of tissue organization (strengthening of axonal or dendritic backbones and surrounding tissue) [56]. We therefore used DTI to investigate tissue microstructure by measuring mean diffusivity (MD), fractional anisotropy (FA), axial diffusivity (AD), radial diffusivity (RD) and mode of anisotropy (MO) that better reflect the integrity of the tissue and its underlying microstructure. To assess hippocampal tissue integrity, we analyzed the SUS- and sham-treated mice by *in vivo* DTI, and compared

group statistical maps of FA, MD, AD and RD and MO between the two groups of animals with an unpaired two-sample t-test using FSL randomize (**Figure 5**). These parameters describe the orientation dependency of water molecules in the intra- and extracellular space suggestive of tissue architecture.

Significant increases in FA values were seen for the hippocampus, prefrontal cortex, thalamus and corpus callosum, revealing more anisotropy of the water motion in the SUS-treated group (**Figure 5A**). FA has been previously been found to be a sensitive measure of brain plasticity following learning [60,61]. An increase in FA value has also been demonstrated to represent myelination [62], together with neurogenesis post-learning or during development [63]. We observed increased FA values in the corpus callosum, which may reflect myelination, whereas those in the gray matter of the hippocampus could be

a result of decreased cell death or neurogenesis. This suggests that SUS treatment may delay the aging process in the brain.

MD values were reduced in the hippocampus after SUS treatment (**Figure 5B**), potentially reflecting reduced cell damage or demyelination compared to the sham group. The latter possibility is supported by studies that have described reduced MD values in the hippocampus and parahippocampal regions after learning [64]. In contrast, MD has been shown to increase in the hippocampus of Alzheimer's patients due to cellular degeneration [65]. In the current study, increases in MD values were also observed in the cortex and posterior part of the hippocampus. Given that MD values reflect structural changes at a microscopic level which facilitate the molecular movement of water, and similar regions show increases in AD measures (which has been shown to reflect the growth of neurons and axons in these tissues) [66], this may explain the increases in MD in the latter regions. The significant increases in AD in the SUS group in both the gray and white matter (**Figure 5C**) may also indicate the growth of neurons and axons in these regions.

The directional diffusivity derived from the DTI measurement describes microscopic water movement parallel (AD) and perpendicular (RD) to axonal tracts.

It has previously been shown in mouse models of white matter injury that an increase in RD is associated with myelin injury [67]. It has also been reported that RD increases with clinical disability and severe tissue injury [68]. In our study, multiple brain regions showed significantly decreased RD (**Figure 5D**). This, together with the associated increase in FA and decrease in MD, suggests an increase in myelin integrity or reduced demyelination in the SUS-treated compared to the sham group.

MO is yet another DTI measure that specifies the type of anisotropy as a continuous measure reflecting differences in the shape of the diffusion tensor ranging from planar (in regions where two fiber populations of similar density cross) to linear (in regions where one fiber orientation predominates). Increases in MO have often been reported in studies of age- or disease-related neurodegeneration [69,70]. We found increases in MO in the cortex of the SUS-treated group, which co-localized with increases in FA. Reduced MO, however, was seen in the amygdala of the SUS-treated mice compared to the sham group.

In conclusion, all measures of diffusion appear to support a potentially neuroprotective effect of ultrasound treatment on the brain, in line with previous observations [32].
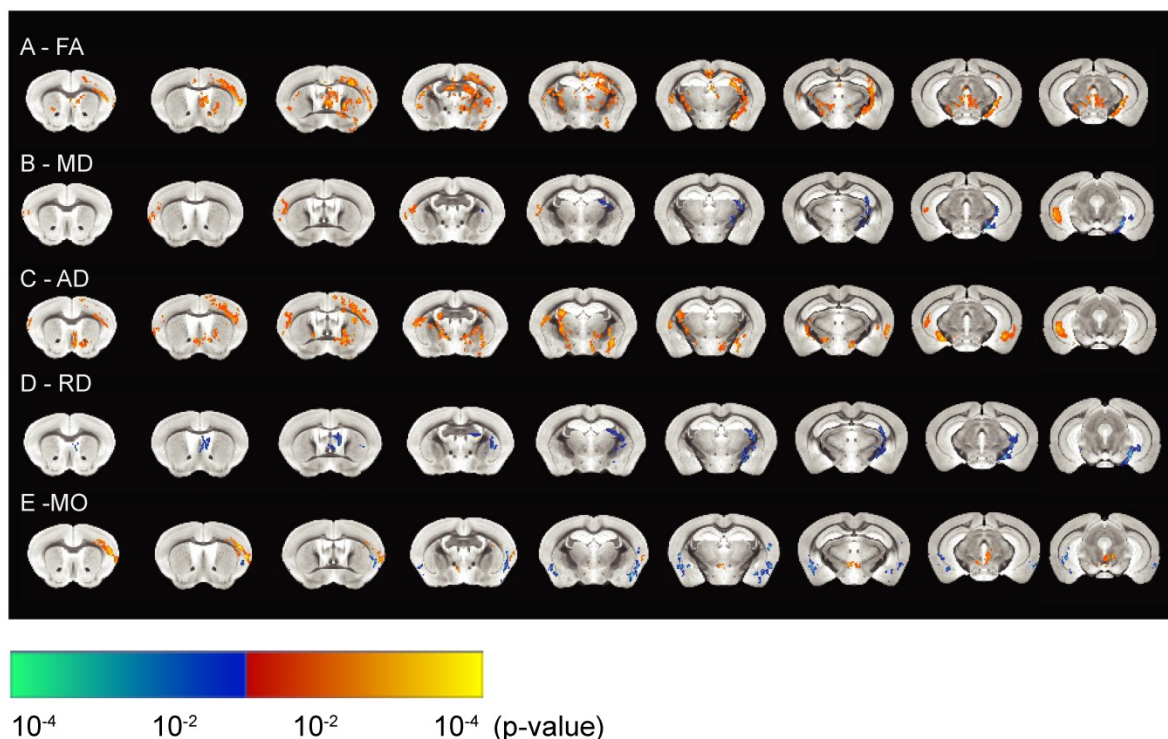

Figure 5. *In vivo* **high-resolution diffusion tensor imaging reveals reduced hippocampal diffusivity in SUS-treated mice. (A)** Fractional anisotropy (FA) maps representing SUS- versus sham-treated mice. **(B)** Maps representing changes in mean diffusivity (MD), **(C)** axial diffusivity (AD), **(D)** radial diffusivity (RD), and **(E)** mode of anisotropy (MO) between SUS- and sham-treated groups. The images represent differences in the group means of the diffusion parameters overlaid on the AMBMC template (p<0.05). The areas in orange represent significant increases in quantitative DTI measures in the SUS group while the areas in blue represent a reduction in this group.

LTP recordings and Golgi staining at 18 months reveal that SUS treatment initiated at 12 months is safe

Neurotransmitters and their receptors are the key modulators of synaptic transmission, and any changes in these components can result in a significant alteration of the physiology of the brain. Such changes can be assessed by electrophysiology, which provides information at a synaptic level of activity. Therefore, we next determined whether SUS treatment has an impact on basal synaptic transmission, using brain slices from mice that had undergone the MRI analysis and were sacrificed at 18 months. The dentate gyrus is the major subregion of the hippocampus that shows functional changes during aging, whereas the CA1 region and the entorhinal cortex are relatively preserved [71,72]. We therefore tested the impact of SUS on perforant path input to the dentate gyrus. Stimulation of the perforant path evoked synaptic inputs that were similar to those in sham-trea ted animals. Neither the decay time constant of evoked excitatory post-synaptic currents (EPSCs) (**Figure 6A**) nor the input-output relationship was altered, demonstrating that neither the overall input nor the basic biophysical properties of these synapses were affected by SUS treatment.

As synaptic LTP is the major cellular model for memory formation in the mammalian brain [73], we next tested the impact of SUS on LTP in the dentate gyrus. Theta burst stimulation of the perforant path input evoked LTP in both SUS- and sham-treated animals that was of a comparable amplitude (SUS: 167.14% ± 15.21%, n=7 slices from 4 mice; sham: 171.73% ± 17.48%, n=8 slices from 5 mice) (**Figure 6B**). This indicates that SUS treatment does not adversely affect glutamatergic synaptic transmission or LTP as a cellular correlate of memory. Our data extend a previous study in which younger wild-type mice were treated with SUS, revealing no adverse effect on the firing properties of neurons in the CA1 sub-region of the hippocampus [32]. Therefore, it is worth noting that demonstration of the safety of the procedure is not limited to a specific area of the hippocampus.
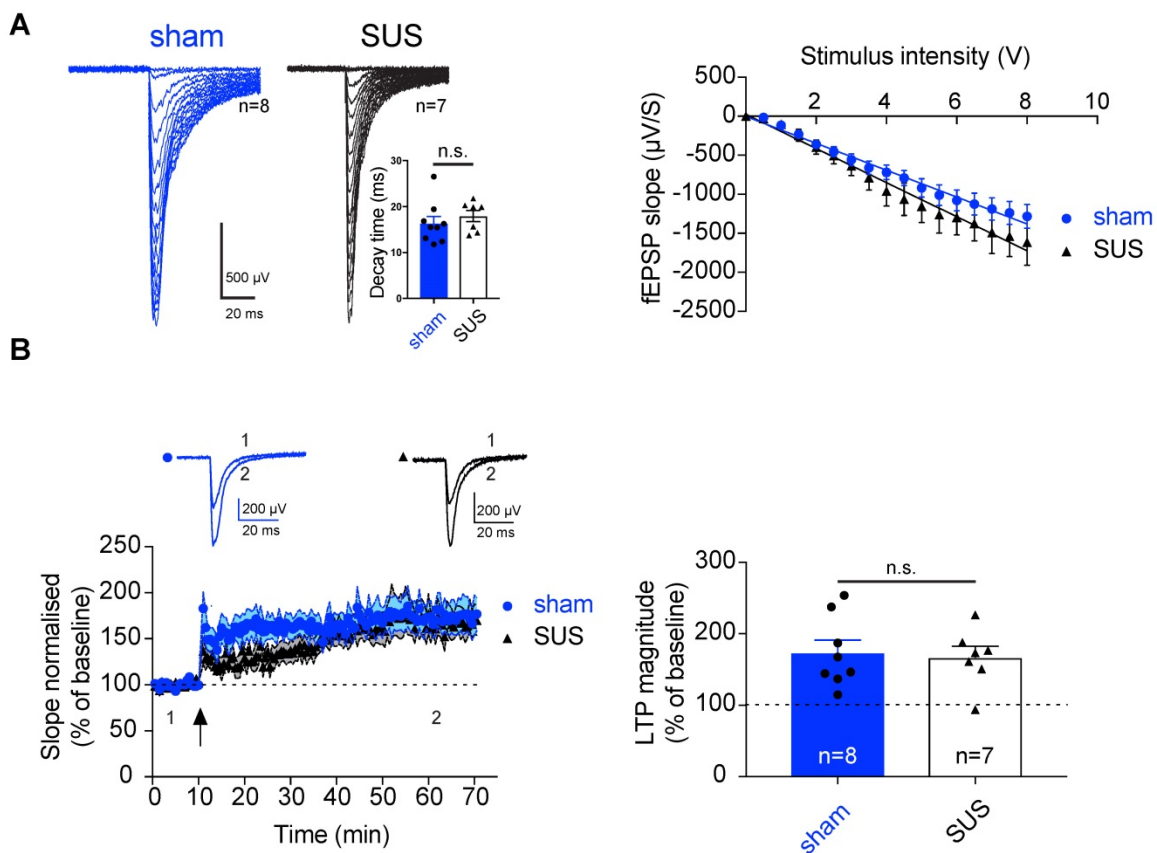

Figure 6. SUS treatment does not affect synaptic transmission and plasticity in the dentate gyrus of 18-month-old mice. (A) Left panels: Representative example of an input/output (I/O) curve for both SUS- and sham-treated mice. Right panels: Average of the I/O for both groups (mean ± SEM). SUS treatment did not change synaptic transmission. Inset: histogram representing the decay time for both SUS- and sham-treated mice. **(B)** Following theta-burst stimulation (TBS) *in vitro* (indicated by a black arrow) robust LTP was observed in both groups (SUS: n=7 slices from 4 mice; sham: n=8 slices from 5 mice, mean ± SEM). Inset: Representative trace before TBS (1), and during the last 10 min of recording (2; average of 20 traces). Right panel: Histogram representing the average of the last 10 min of LTP (mean ± SEM). fEPSPs: field excitatory post-synaptic potentials.
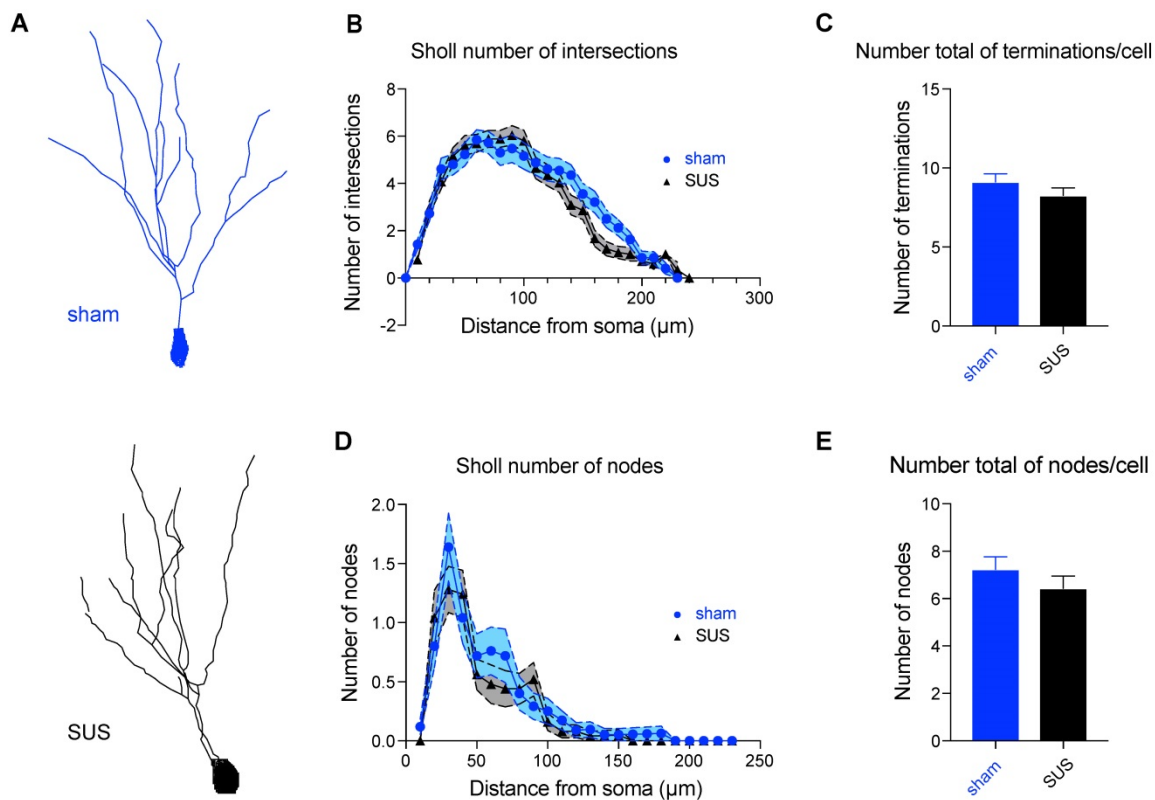
Figure 7. SUS treatment does not modify neuronal morphology in the dentate gyrus. (A) Representative 3D reconstruction of a SUS- and a sham-treated neuron. **(B)** Sholl analysis displaying the number of intersections and revealing no changes in ramification of neuronal processes, displayed as a function of the distance from the soma in Golgi-impregnated neurons from SUS- and sham-treated mice, **(C)** the total number of terminals per cell, **(D)** the node distribution over the dendrites, and **(E)** the total number of nodes per cell (3 mice per group, 25 neurons per group).

Synaptic transmission is finely modulated by the structural anatomy of neurons. Golgi staining was therefore performed, which allowed us to randomly stain neurons in brain tissues and study their dendritic tree (**Figure 7A**). In line with the absence of any impairment in synaptic transmission, we found no difference in a Sholl analysis (analyzing 3 mice and 25 neurons for each group). No morphological differences were revealed between the two groups, as the number of intersections (**Figure 7B**), the total number of terminals per cell (**Figure 7C**), the node distribution over the dendrites (**Figure 7D**), and the total number of nodes per cell (**Figure 7E**) were all similar.

Conclusion

In this study, we assessed the effects of SUS treatment on neuronal function in aged mice, treating 12-month-old animals with six weekly SUS sessions (up to 13.5 months of age, using sham treatments as control), followed by sacrifice at 18 months of age. A limitation of our study is that although we used 18-month-old mice, which in humans equates to 60-65 years of age, mice at a very advanced age have not been analyzed, although this is difficult to implement as older animals become increasingly susceptible to repeated manipulations. By assessing the mice in the APA test at 12, 15 and 18 months, we found that spatial learning and memory were not negatively affected by SUS treatment. Field recordings performed at 18 months revealed that SUS treatment also had no adverse effect on glutamatergic synaptic transmission and LTP. Golgi staining followed by Sholl analysis did not reveal morphological differences, thereby supporting our electrophysiological results. MRS revealed no significant differences between the two groups specifically in the hippocampus. Finally, measures of diffusion as determined by DTI, were suggestive of a potentially protective effect of SUS treatment on the brain.

Together, our data expand upon the body of safety work that has been conducted to date, which predominantly used classical histological techniques and MRI, and as far as mice are concerned, relatively younger animals. To our knowledge, the long-term effects of ultrasound-mediated BBB opening has previously not been addressed by such a range of analysis tools, which in our study in aged mice encompassed the APA test as a cognitive read-out, Golgi stains to reveal neuronal morphology, LTP as an electrophysiological correlate of memory, and the

imaging techniques MRI, MRS and DTI. Our comprehensive, multimodal analysis in rodents adds to the notion that ultrasound is a highly tunable modality that is safe long-term, underscoring its potential to be developed into a novel treatment strategy for diseases of the brain. More specifically, our results show that it is safe to apply repeated SUS even in a population of mice that is susceptible to natural cognitive decline due to the aging process.

Abbreviations

3D: three-dimensional; aCSF: artificial cerebrospinal fluid; AD: axial diffusivity; AMBMC: Australian Mouse Brain Mapping Consortium; Aβ: amyloid-β; APA: active place avoidance; BBB: blood-brain barrier; DTI: diffusion tensor imaging; Dtifit: diffusion toolkit; EPSC: evoked excitatory post-synaptic current; FA: fractional anisotropy; FLIRT: FMRIB linear co-registration tool; FMRIB: functional magnetic resonance imaging of the brain; FSL: FMRIB software library; FNIRT: FMRIB nonlinear co-registration tool; H&E: hematoxylin and eosin; HPLC: high-performance liquid chromatography; LTP: long-term potentiation; MD: mean diffusivity; MO: mode of anisotropy; MRI: magnetic resonance imaging; MRS: magnetic resonance spectroscopy; OVS: outer volume saturation; PCNN: pulse-coupled neural networks; PFA: paraformaldehyde; PRESS: point-resolved spectroscopy; RD: radial diffusivity; SUS: scanning ultrasound; TBS: theta-burst stimulation; TcMRgFUS: transcranial magnetic resonance-guided focused ultrasound; TIPS: Therapy Imaging Probe System; VAPOR: variable power radio frequency pulses with an optimized relaxation delay; VBM: voxel-based morphometry.

Supplementary Material

Supplementary figures.
http://www.thno.org/v08p6233s1.pdf

Acknowledgements

Competing Interests

The authors have declared that no competing interest exists.

References

1. Leinenga G, Langton C, Nisbet R, and Götz J. Ultrasound treatment of neurological diseases - current and emerging applications. Nat Rev Neurol 2016; 12: 161-174.
2. Appis AW, Tracy MJ, and Feinstein SB. Update on the safety and efficacy of commercial ultrasound contrast agents in cardiac applications. Echo Res Pract 2015; 2: R55-62.
3. McDannold N, Vykhodtseva N, and Hynynen K. Blood-brain barrier disruption induced by focused ultrasound and circulating preformed microbubbles appears to be characterized by the mechanical index. Ultrasound Med Biol 2008; 34: 834-840.
4. Baseri B, Choi JJ, Tung YS, and Konofagou EE. Multi-modality safety assessment of blood-brain barrier opening using focused ultrasound and definity microbubbles: a short-term study. Ultrasound Med Biol 2010; 36: 1445-1459.
5. Chu PC, Chai WY, Tsai CH, et al. Focused ultrasound-induced blood-brain barrier opening: association with mechanical index and cavitation index analyzed by dynamic contrast-enhanced magnetic-resonance imaging. Sci Rep 2016; 6: 33264.
6. Fan CH, Liu HL, Ting CY, et al. Submicron-bubble-enhanced focused ultrasound for blood-brain barrier disruption and improved CNS drug delivery. PLoS One 2014; 9: e96327.
7. Choi JJ, Selert K, Gao Z, et al. Noninvasive and localized blood-brain barrier disruption using focused ultrasound can be achieved at short pulse lengths and low pulse repetition frequencies. J Cereb Blood Flow Metab 2011; 31: 725-737.
8. McDannold N, Vykhodtseva N, and Hynynen K. Effects of acoustic parameters and ultrasound contrast agent dose on focused-ultrasound induced blood-brain barrier disruption. Ultrasound Med Biol 2008; 34: 930-937.
9. O'Reilly MA, Waspe AC, Ganguly M, and Hynynen K. Focused-ultrasound disruption of the blood-brain barrier using closely-timed short pulses: influence of sonication parameters and injection rate. Ultrasound Med Biol 2011; 37: 587-594.
10. Choi JJ, Feshitan JA, Baseri B, et al. Microbubble-size dependence of focused ultrasound-induced blood-brain barrier opening in mice in vivo. IEEE Trans Biomed Eng 2010; 57: 145-154.
11. Choi JJ, Pernot M, Small SA, and Konofagou EE. Noninvasive, transcranial and localized opening of the blood-brain barrier using focused ultrasound in mice. Ultrasound Med Biol 2007; 33: 95-104.
12. Choi JJ, Pernot M, Brown TR, et al. Spatio-temporal analysis of molecular delivery through the blood-brain barrier using focused ultrasound. Phys Med Biol 2007; 52: 5509-5530.
13. Choi JJ, Selert K, Vlachos F, et al. Noninvasive and localized neuronal delivery using short ultrasonic pulses and microbubbles. Proc Natl Acad Sci U S A 2011; 108: 16539-16544.
14. Kinoshita M, McDannold N, Jolesz FA, and Hynynen K. Noninvasive localized delivery of Herceptin to the mouse brain by MRI-guided focused ultrasound-induced blood-brain barrier disruption. Proc Natl Acad Sci U S A 2006; 103: 11719-11723.
15. Leinenga G, and Götz J. Scanning ultrasound removes amyloid-beta and restores memory in an Alzheimer's disease mouse model. Sci Transl Med 2015; 7: 278ra233.
16. Gauthier S, Albert M, Fox N, et al. Why has therapy development for dementia failed in the last two decades? Alzheimers Dement 2016; 12: 60-64.
17. Polanco JC, Li C, Bodea LG, et al. Amyloid-beta and tau complexity - towards improved biomarkers and targeted therapies. Nat Rev Neurol 2018; 14: 22-39.
18. Jordao JF, Thevenot E, Markham-Coultes K, et al. Amyloid-beta plaque reduction, endogenous antibody delivery and glial activation by brain-targeted, transcranial focused ultrasound. Exp Neurol 2013; 248: 16-29.
19. Burgess A, Dubey S, Yeung S, et al. Alzheimer disease in a mouse model: MR imaging-guided focused ultrasound targeted to the hippocampus opens the blood-brain barrier and improves pathologic abnormalities and behavior. Radiology 2014; 273: 736-745.
20. Nisbet RM, van der Jeugd A, Leinenga G, et al. Combined effects of scanning ultrasound and a tau-specific single chain antibody in a tau transgenic mouse model. Brain 2017; 140: 1220-1230.
21. Leinenga G, and Götz J. Safety and efficacy of scanning ultrasound treatment of aged APP23 mice. Front Neurosci 2018; 743.
22. Jordao JF, Ayala-Grosso CA, Markham K, et al. Antibodies targeted to the brain with image-guided focused ultrasound reduces amyloid-beta plaque load in the TgCRND8 mouse model of Alzheimer's disease. PLoS One 2010; 5: e10549.

23. Olumolade OO, Wang S, Samiotaki G, and Konofagou EE. Longitudinal motor and behavioral assessment of blood-brain barrier opening with transcranial focused ultrasound. Ultrasound Med Biol 2016; 42: 2270-2282.

24. Yang FY, Lin YS, Kang KH, and Chao TK. Reversible blood-brain barrier disruption by repeated transcranial focused ultrasound allows enhanced extravasation. J Control Release 2011; 150: 111-116.

25. O'Reilly MA, Jones RM, Barrett E, et al. Investigation of the safety of focused ultrasound-induced blood-brain barrier opening in a natural canine model of aging. Theranostics 2017; 7: 3573-3584.

26. Pelekanos M, Leinenga G, Odabaee M, et al. Establishing sheep as an experimental species to validate ultrasound-mediated blood-brain barrier opening for potential therapeutic interventions. Theranostics 2018; 8: 2583-2602.

27. McDannold N, Arvanitis CD, Vykhodtseva N, and Livingstone MS. Temporary disruption of the blood-brain barrier by use of ultrasound and microbubbles: safety and efficacy evaluation in rhesus macaques. Cancer Res 2012; 72: 3652-3663.

28. Downs ME, Buch A, Karakatsani ME, et al. Blood-brain barrier opening in behaving non-human primates via focused ultrasound with systemically administered microbubbles. Sci Rep 2015; 5: 15076.

29. Lipsman N, Meng Y, Bethune AJ, et al. Blood-brain barrier opening in Alzheimer's disease using MR-guided focused ultrasound. Nat Commun 2018; 9: 2336.

30. Kovacs ZI, Kim S, Jikaria N, et al. Disrupting the blood-brain barrier by focused ultrasound induces sterile inflammation. Proc Natl Acad Sci U S A 2017; 114: E75-E84.

31. McMahon D, and Hynynen K. Acute inflammatory response following increased blood-brain barrier permeability induced by focused ultrasound is dependent on microbubble dose. Theranostics 2017; 7: 3989-4000.

32. Hatch RJ, Leinenga G, and Götz J. Scanning ultrasound (SUS) causes no changes to neuronal excitability and prevents age-related reductions in hippocampal CA1 dendritic structure in wild-type mice. PLoS One 2016; 11: e0164278.

33. Benice TS, Rizk A, Kohama S, et al. Sex-differences in age-related cognitive decline in C57BL/6J mice associated with increased brain microtubule-associated protein 2 and synaptophysin immunoreactivity. Neuroscience 2006; 137: 413-423.

34. Carlesimo GA, Piras F, Orfei MD, et al. Atrophy of presubiculum and subiculum is the earliest hippocampal anatomical marker of Alzheimer's disease. Alzheimers Dement (Amst) 2015; 1: 24-32.

35. Seip R, Chin CT, Hall CS, et al. Targeted ultrasound-mediated delivery of nanoparticles: on the development of a new HIFU-based therapy and imaging device. IEEE Trans Biomed Eng 2010; 57: 61-70.

36. Vukovic J, Borlikova GG, Ruitenberg MJ, et al. Immature doublecortin-positive hippocampal neurons are important for learning but not for remembering. J Neurosci 2013; 33: 6603-6613.

37. Chou N, Wu J, Bai Bingren J, et al. Robust automatic rodent brain extraction using 3-D pulse-coupled neural networks (PCNN). IEEE Trans Image Process 2011; 20: 2554-2564.

38. Tustison NJ, and Avants BB. Explicit B-spline regularization in diffeomorphic image registration. Front Neuroinform 2013; 7: 39.

39. Jenkinson M, Bannister P, Brady M, and Smith S. Improved optimization for the robust and accurate linear registration and motion correction of brain images. Neuroimage 2002; 17: 825-841.

40. Jenkinson M, and Smith S. A global optimisation method for robust affine registration of brain images. Med Image Anal 2001; 5: 143-156.

41. Klein A, Andersson J, Ardekani BA, et al. Evaluation of 14 nonlinear deformation algorithms applied to human brain MRI registration. Neuroimage 2009; 46: 786-802.

42. Richards K, Watson C, Buckley RF, et al. Segmentation of the mouse hippocampal formation in magnetic resonance images. Neuroimage 2011; 58: 732-740.

43. Ullmann JF, Keller MD, Watson C, et al. Segmentation of the C57BL/6J mouse cerebellum in magnetic resonance images. Neuroimage 2012; 62: 1408-1414.

44. Badea A, Ali-Sharief AA, and Johnson GA. Morphometric analysis of the C57BL/6J mouse brain. Neuroimage 2007; 37: 683-693.

45. Behrens TE, Woolrich MW, Jenkinson M, et al. Characterization and propagation of uncertainty in diffusion-weighted MR imaging. Magn Reson Med 2003; 50: 1077-1088.

46. Provencher SW. Estimation of metabolite concentrations from localized in vivo proton NMR spectra. Magn Reson Med 1993; 30: 672-679.

47. Winkler AM, Ridgway GR, Webster MA, et al. Permutation inference for the general linear model. Neuroimage 2014; 92: 381-397.

48. Das G, Reuhl K, and Zhou R. The Golgi-Cox method. Methods Mol Biol 2013; 1018: 313-321.

49. Harrison FE, Hosseini AH, and McDonald MP. Endogenous anxiety and stress responses in water maze and Barnes maze spatial memory tasks. Behav Brain Res 2009; 198: 247-251.

50. van Praag H, Shubert T, Zhao C, and Gage FH. Exercise enhances learning and hippocampal neurogenesis in aged mice. J Neurosci 2005; 25: 8680-8685.

51. Su L, Hayes L, Soteriades S, et al. Hippocampal stratum radiatum, lacunosum, and moleculare sparing in mild cognitive impairment. J Alzheimers Dis 2018; 61: 415-424.

52. Perluigi M, Swomley AM, and Butterfield DA. Redox proteomics and the dynamic molecular landscape of the aging brain. Ageing Res Rev 2014; 13: 75-89.

53. Lessard-Beaudoin M, Laroche M, Demers MJ, et al. Characterization of age-associated changes in peripheral organ and brain region weights in C57BL/6 mice. Exp Gerontol 2015; 63: 27-34.

54. Marjanska M, Curran GL, Wengenack TM, et al. Monitoring disease progression in transgenic mouse models of Alzheimer's disease with proton magnetic resonance spectroscopy. Proc Natl Acad Sci U S A 2005; 102: 11906-11910.

55. Chen SQ, Wang PJ, Ten GJ, et al. Role of myo-inositol by magnetic resonance spectroscopy in early diagnosis of Alzheimer's disease in APP/PS1 transgenic mice. Dement Geriatr Cogn Disord 2009; 28: 558-566.

56. Assaf Y, and Pasternak O. Diffusion tensor imaging (DTI)-based white matter mapping in brain research: a review. J Mol Neurosci 2008; 34: 51-61.

57. Scholz J, Klein MC, Behrens TE, and Johansen-Berg H. Training induces changes in white-matter architecture. Nat Neurosci 2009; 12: 1370-1371.

58. Barazany D, Basser PJ, and Assaf Y. In vivo measurement of axon diameter distribution in the corpus callosum of rat brain. Brain 2009; 132: 1210-1220.

59. Blumenfeld-Katzir T, Pasternak O, Dagan M, and Assaf Y. Diffusion MRI of structural brain plasticity induced by a learning and memory task. PLoS One 2011; 6: e20678.

60. Engvig A, Fjell AM, Westlye LT, et al. Memory training impacts short-term changes in aging white matter: a longitudinal diffusion tensor imaging study. Hum Brain Mapp 2012; 33: 2390-2406.

61. Lövdén M, Wenger E, Martensson J, et al. Structural brain plasticity in adult learning and development. Neurosci Biobehav Rev 2013; 37: 2296-2310.

62. Song SK, Sun SW, Ramsbottom MJ, et al. Dysmyelination revealed through MRI as increased radial (but unchanged axial) diffusion of water. Neuroimage 2002; 17: 1429-1436.

63. Schadl K, Vassar R, Cahill-Rowley K, et al. Prediction of cognitive and motor development in preterm children using exhaustive feature selection and cross-validation of near-term white matter microstructure. Neuroimage Clin 2018; 17: 667-679.

64. Sagi Y, Tavor I, Hofstetter S, et al. Learning in the fast lane: new insights into neuroplasticity. Neuron 2012; 73: 1195-1203.

65. Hong YJ, Yoon B, Shim YS, et al. Differences in microstructural alterations of the hippocampus in Alzheimer disease and idiopathic normal pressure hydrocephalus: a diffusion tensor imaging study. Am J Neuroradiol 2010; 31: 1867-1872.

66. Naismith SL, Redoblado-Hodge MA, Lewis SJ, et al. Cognitive training in affective disorders improves memory: a preliminary study using the NEAR approach. J Affect Disord 2010; 121: 258-262.

67. Budde MD, Kim JH, Liang HF, et al. Toward accurate diagnosis of white matter pathology using diffusion tensor imaging. Magn Reson Med 2007; 57: 688-695.

68. Klawiter EC, Schmidt RE, Trinkaus K, et al. Radial diffusivity predicts demyelination in ex vivo multiple sclerosis spinal cords. Neuroimage 2011; 55: 1454-1460.

69. Sullivan EV, and Pfefferbaum A. Diffusion tensor imaging and aging. Neurosci Biobehav Rev 2006; 30: 749-761.

70. Bozzali M, and Cherubini A. Diffusion tensor MRI to investigate dementias: a brief review. Magn Reson Imaging 2007; 25: 969-977.

71. Yassa MA, Muftuler LT, and Stark CE. Ultrahigh-resolution microstructural diffusion tensor imaging reveals perforant path degradation in aged humans in vivo. Proc Natl Acad Sci U S A 2010; 107: 12687-12691.

72. Small SA, Schobel SA, Buxton RB, et al. A pathophysiological framework of hippocampal dysfunction in ageing and disease. Nat Rev Neurosci 2011; 12: 585-601.

73. Poo MM, Pignatelli M, Ryan TJ, et al. What is memory? The present state of the engram. BMC Biol 2016; 14: 40.